ADVANCED FUNCTIONAL MATERIALS
www.afm-journal.de

Highly Porous Polymer Aerogel Film-Based Triboelectric Nanogenerators

*Qifeng Zheng, Liming Fang, Haiquan Guo, Kefang Yang, Zhiyong Cai, Mary Ann B. Meador, and Shaoqin Gong**

A novel class of high performance polymer porous aerogel film-based triboelectric nanogenerators (A-NGs) is demonstrated. The A-NGs, made of a pair of highly porous polymer films, exhibit much higher triboelectric outputs than the corresponding dense polymer film-based triboelectric nanogenerators (D-NGs) under the same mechanical stress. The triboelectric outputs of the A-NGs increase significantly with increasing porosity, which can be attributed to the increase in contact area and the electrostatic induction in the porous structure, thereby leading to additional charges on the porous surface. Remarkably, the A-NG fabricated using porous chitosan aerogel film paired with the most porous polyimide (with a porosity of 92%) aerogel film demonstrates a very high voltage of 60.6 V and current of 7.7 μA, corresponding to a power density of 2.33 W m^{-2}, which is sufficient to power 22 blue light-emitting-diodes (LEDs). This is the first report on triboelectric nanogenerators (TENGs) employing porous polymer aerogel films as both positive and negative materials to enhance triboelectric outputs. Furthermore, enhancing the tribopositive polarity of the cellulose aerogel film via silanization using aminosilane can dramatically improve the triboelectric performance. Therefore, this study provides new insights into investigating porous materials with tunable triboelectric polarities for high performance TENGs.

1. Introduction

With the rapid expansion of the global economy, limited availability of fossil fuels, and increasing environmental pollution, there is a growing demand for efficient, clean, and sustainable sources of energy.[1] Nanogenerators (NGs), a new class of clean and sustainable energy harvesting devices capable of harvesting energy from the ambient environment—such as light, heat, and mechanical vibrations—have been extensively investigated during the last decade.[2–5] Among them, triboelectric nanogenerators (TENGs) have been recognized as a novel and promising technology for harvesting ubiquitous mechanical energy from the natural environment due to their high efficiency, high output power, low cost, and ease of manufacturing.[2,6]

The working principle of TENGs is based on the coupling effect of the triboelectric effect and electrostatic induction.[2,6,7] Specifically, energy conversion of TENGs is achieved by surface charge transfer resulting from periodic contact between two dissimilar materials in a triboelectric series that differ in tribopolarity. Thus, TENGs generally consist of two materials that have distinct electron affinities, which are termed positive and negative materials. The most common positive materials used in TENGs are metals (e.g., Ag and Cu) and metal oxides (e.g., ZnO and indium tin oxide (ITO)). Some common negative materials include fluorinated

Dr. Q. Zheng, Dr. L. Fang, Dr. K. Yang, Prof. S. Gong
Department of Material Science and Engineering
University of Wisconsin–Madison
Madison, WI 53706, USA
E-mail: shaoqingong@wisc.edu
Dr. Q. Zheng, Dr. L. Fang, Dr. K. Yang, Prof. S. Gong
Wisconsin Institutes for Discovery
University of Wisconsin–Madison
Madison, WI 53715, USA
Dr. Q. Zheng, Dr. L. Fang, Dr. K. Yang, Prof. S. Gong
Department of Biomedical Engineering
University of Wisconsin–Madison
Madison, WI 53706, USA
Dr. L. Fang
School of Materials Science and Engineering
South China University of Technology
Guangzhou 510641, P. R. China
Dr. H. Guo
Ohio Aerospace Institute
Brookpark, OH 44142, USA
Dr. K. Yang
Key Laboratory of Organosilicon Chemistry and Material Technology of Education
Hangzhou Normal University
Hangzhou 311121, P. R. China
Dr. Z. Cai
Forest Products Laboratory
USDA
Madison, WI 53726, USA
Dr. M. A. B. Meador
NASA Glenn Research Center
Cleveland, OH 44135, USA
The ORCID identification number(s) for the author(s) of this article can be found under https://doi.org/10.1002/adfm.201706365.

DOI: 10.1002/adfm.201706365

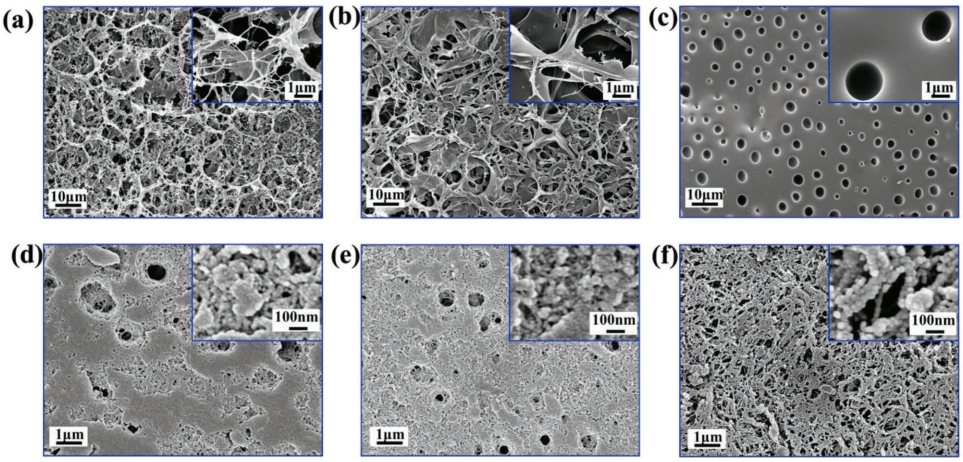

Figure 1. SEM images of the bottom surfaces of various porous polymer films: a) P-CNF aerogel, b) P-CTS aerogel, c) P-PDMS sponge, d) P-PI78 aerogel, e) P-PI84 aerogel, and f) P-PI92 aerogel.

ethylene propylene, polyvinylidene fluoride, polydimethylsiloxane (PDMS), polytetrafluoroethylene (PTFE), polyimide (PI), and polyethylene terephthalate (PET).[2,6,8–14] However, metal-based positive materials can be easily oxidized or corroded in a harsh environment,[15] which can dramatically affect the long-term stability of the resulting TENGs. Alternatively, polymeric materials, which have good shape adaptability,[16] such as polyamide,[17] cellulose,[18,19] and polypyrrole (PPy),[15,20] have been investigated for use as positive materials for TENGs. For instance, Wang et al.[15] developed an all-polymer-based TENG fabricated using polypyrrole as the positive material paired with PTFE as the negative material. This TENG demonstrated an open-circuit voltage (V_{oc}) of 48 V and a short-circuit current (I_{sc}) of up to 30 mA m^{-2}, corresponding to a power density of 1.44 W m^{-2}. However, these polymer-based positive materials generally exhibit lower triboelectric performance than their metal-based counterparts when used to assemble TENGs. Thus, achieving high triboelectric performance has been a great challenge for all-polymer-based TENGs.

Cellulose and its derivatives are polysaccharides, the most abundant natural polymers on earth, and are renewable, biocompatible, and biodegradable.[21] Cellulose nanofibrils (CNFs)[22,23] derived from cellulose have high aspect ratios, high transparency, excellent mechanical properties, excellent flexibility, and desirable electrical properties.[22,23] They have been increasingly explored as flexible energy storage and harvesting materials.[22,24–28] Due to its tendency to lose electrons, cellulose has been considered as a positive material in the triboelectric series.[6,13] However, natural cellulose only exhibits weak tribopolarity, which results in inferior performance when used to assemble TENGs.[29] Chitosan (CTS) is a polysaccharide that consists of β-1,4-D-linked glucosamine units.[30] In the presence of amino groups, which have excellent electron-donating functionality,[31] CTS is expected to exhibit much higher tribopositive polarity compared to natural cellulose, which makes CTS an ideal candidate as a positive material for fabricating TENGs.

Herein, we report a new type of high performance A-NG consisting of a pair of highly porous polymer aerogel films that exhibits significant and stable triboelectric power outputs. Highly porous CNF and CTS aerogels (P-CNF and P-CTS) were employed as triboelectric positive materials paired with porous polydimethylsiloxane (P-PDMS), a well-known triboelectric negative material, to assemble P-CNF/P-PDMS and P-CTS/P-PDMS paired A-NGs. The resulting P-CNF/P-PDMS and P-CTS/P-PDMS paired A-NGs exhibited an 8-fold and 11-fold power enhancement, respectively, compared to the corresponding dense film-based TENGs (D-NGs) under the same mechanical stress. Furthermore, the effects of aerogel porosity on the triboelectric performance of A-NGs were also investigated using porous CNF and CTS aerogels paired with porous polyimide aerogels (P-PI) with various porosities. These systematic studies have demonstrated that the output voltage and current of A-NGs increased with increasing porosity and Brunauer–Emmett–Teller (BET) surface area of the polymer aerogel. This is the first report that porous CNF and CTS aerogels can be used as triboelectric positive materials to enhance the output performance of TENGs. In addition, we have demonstrated that the tribopositive polarity of cellulose can be improved via surface functionalization of cellulose with aminosilane, leading to a dramatically enhanced TENG output performance. Our approach using highly porous polymer films as both triboelectric positive and negative layers will provide new insights into designing new materials for fabricating high performance and low cost energy harvesting devices.

2. Results and Discussion

Highly porous CNF and CTS aerogels were prepared using an environmental friendly freeze-drying process as reported previously (detailed information is described in the Experimental Section).[32,33] The CNF and CTS aerogel films were obtained by compressing the aerogel at 1.0 MPa. As shown in **Figure 1**a, the porous CNF aerogel film (P-CNF) exhibited an interconnected, highly porous, and nanofiber-like structure. This was attributed to the high aspect ratios of CNFs, thereby allowing CNFs to easily entangle and form a 3D network.[32,33] The P-CTS aerogel film also displayed a highly porous and interconnected structure

(Figure 1b).[34] Figure S1a,b in the Supporting Information shows the cross-section scanning electron microscope (SEM) images of the P-CNF and P-CTS aerogel films, from which well stacked layers can be observed. Figure 1c shows the P-PDMS sponge (porosity: 32%) with relatively uniform pore sizes of ≈3 µm, which was prepared using a solvent evaporation induced phase separation method.[35] Furthermore, three PI aerogels with varied porosities were also prepared as triboelectric negative materials. PI aerogels were synthesized by crosslinking biphenyl-3,3',4,4'-tetracarboxylic dianydride (BPDA) with 50% 2,2'-dimethylbenzidine (DMBZ) and 50% 4,4'-oxydianiline (ODA), followed by supercritical drying or air drying as previous described.[36] Three porous PI aerogels with a porosity of 78%, 84%, and 92% were termed as P-PI78, P-PI84, and P-PI92, respectively. Figure 1f shows the SEM image of the bottom surface of the PI aerogel film made by supercritical drying (i.e., P-PI92), which formed a 3D network of entangled polymer nanofibers.[36] This is in contrast to PI aerogels made by air drying (i.e., P-PI78 and P-PI84) that had less open porosity, which may be attributed to the solvent evaporation causing a greater collapse of the pores. However, as shown in the cross-section SEM images (Figure S1d–f, Supporting Information), the interior of all of the aerogel films had a fiber-like structure and relative bigger and more numerous pores. Nevertheless, the supercritically dried P-PI92 had a finer, fiber-like structure as compared to either of the air dried samples.

All of the porous polymer films—including P-CNF, P-CTS, P-PDMS, and all three PI aerogels—were mechanically robust and highly flexible. P-CNF, P-CTS, and the P-PI aerogels exhibited densities below 0.4 g cm^{-3} and porosities of around 80% or more. The most porous PI aerogel, P-PI92, also possessed a high BET surface area (**Table 1**). As illustrated in **Figure 2**a, the P-CNF or P-CTS was used as the triboelectric positive layer, and P-PDMS or P-PI was employed as the triboelectric negative layer, to assemble various A-NGs. Both positive and negative layers of the same size (1 cm × 2 cm) were attached on a flexible ITO/PET substrate, with the distance between the two substrates fixed at 2 mm for all tests. The as-fabricated A-NGs were highly flexible (Figure 2b). To compare the triboelectric outputs and verify the advantages of highly porous aerogel films over dense films, D-NGs were fabricated using either dense CNF (D-CNF) or dense CTS (D-CTS) film paired with dense PDMS (D-PDMS) film of the same dimension (i.e., 1 cm × 2 cm).

Table 1. Physical properties of various porous polymer films.

Sample	Density [g cm^{-3}]	Porosity [%]	BET surface area [m^2 g^{-1}]
P-CNF	0.227 ± 0.005	84	68
P-CTS	0.245 ± 0.004	86	43
P-PDMS	0.652 ± 0.013	32	8.8
P-PI78	0.397 ± 0.033	78	47
P-PI84	0.292 ± 0.032	84	66
P-PI92	0.185 ± 0.003	92	212

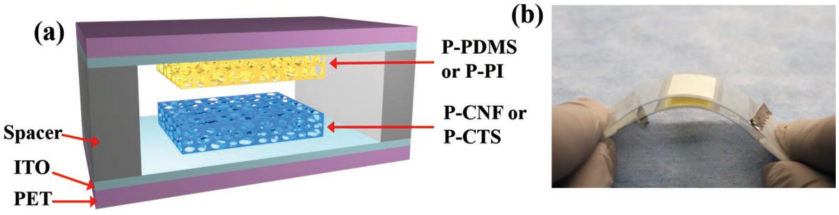

Figure 2. a) A schematic diagram and b) a photograph of a highly porous aerogel film-based TENG (A-NG).

Figure 3a,b presents the typical output voltage and current generated by the D-NGs fabricated using D-CNF paired with D-PDMS, and A-NGs fabricated using P-CNF paired with P-PDMS under a periodic force of ≈6 N (i.e., 0.03 MPa) at a frequency of 10 Hz. As shown in Figure 3a,b, the output voltage and current generated by D-CNF/D-PDMS paired D-NG were 7.6 V and 0.8 µA, respectively, with a corresponding power density of 0.03 W m^{-2}. In contrast, the output voltage and current generated by the P-CNF/P-PDMS A-NG were 22.3 V and 2.2 µA, respectively, with a corresponding power density of 0.25 W m^{-2}, indicating an eightfold power density enhancement relative to the D-NG. For comparison, the output performance of one dense-film and one porous-film-paired TENGs (i.e., P-CNF/D-PDMS TENG and D-CNF/P-PDMS TENG) were also investigated. As shown in Figure S2 in the Supporting Information, the P-CNF/D-PDMS and D-CNF/P-PDMS TENGs showed an output voltage of 16.6 and 16.0 V, respectively, which was higher than that of the D-CNF/D-PDMS D-NG (i.e., 7.6 V), but lower than that of the P-CNF/P-PDMS A-NG (i.e., 22.3 V).

The triboelectric power generation mechanism, as previously demonstrated, is based on the coupling effect of triboelectric effect and electrostatic induction.[2,6] As shown in **Figure 4**aI, before the contact of the triboelectric pair (i.e., D-CNF and D-PDMS in present case), there is no charge generated, thus there is no electrical potential difference. When the two polymer films are brought into contact under a mechanical force, surface charge transfer occurs; namely, the electrons are injected from CNF to PDMS, resulting in positive charges on the surface of the CNF and negative charges on the surface of the PDMS (Figure 4aII). As the TENG starts to release, an electrical potential difference between the top and bottom electrodes is established, thereby driving the electrons to flow from the top electrode to the bottom electrode through the external circuit, resulting in an electric output signal (Figure 4aIII,IV). When the TENG is under pressure again, the reduction of the interlayer distance makes the top electrode possess a higher electric potential that leads to the backflow of electrons from the bottom electrode to the top electrode through the external circuit, leading to reverse electrical signals (Figure 4aV).

However, in the case of a porous polymer film-based A-NG (i.e., P-CNF and P-PDMS in the present case), the charges are not only induced on the contact surface upon contact, additional charges on the porous surface of P-CNF and P-PDMS will also be generated owing to the compression of pores with the associated electrostatic effects (Figure 4bII), resulting in a larger electrical potential difference between the top and

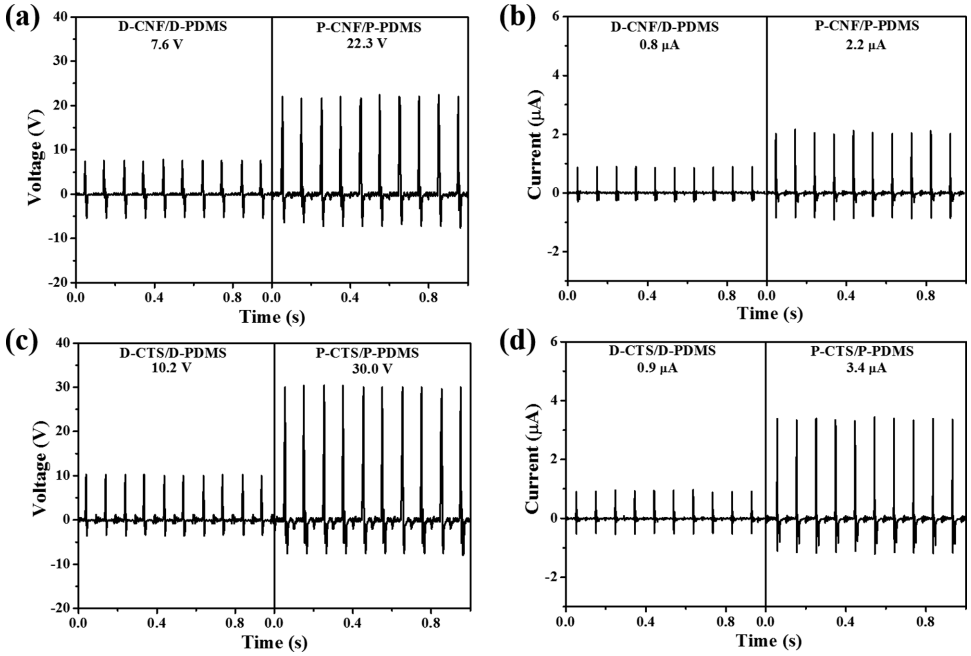

Figure 3. Comparison of the triboelectric output voltage and current generated by various D-NGs and A-NGs. Output a) voltage and b) current generated by the D-NG fabricated using D-CNF paired with D-PDMS and A-NG fabricated using P-CNF paired with P-PDMS. Output c) voltage and d) current generated by the D-NG fabricated using D-CTS paired with D-PDMS and A-NG fabricated using P-CTS paired with P-PDMS.

bottom electrodes upon release (Figure 4bIII), thereby leading to a much higher electrical output compared to D-CNF/D-PDMS D-NGs.[37,38] Furthermore, the porous polymer films exhibited a higher deformation compared to the dense films under the same compressive stress, which will increase the relative capacitance, thus increasing the triboelectric output.[37,39] Lee et al.[37] reported a sponge PDMS/Al TENG that exhibited an enhanced output performance compared to the flat PDMS film-based TENG. This was attributed to the additional triboelectric charges generated on the surface of the inner pores by electrostatic induction as well as a notable capacitance change under mechanical stress.

Figure 3c,d shows the output voltage and current generated by the D-CTS/D-PDMS D-NG and P-CTS/P-PDMS A-NG. Similar to what was observed for TENG employing CNF as the triboelectric positive layer, the P-CTS/P-PDMS A-NG exhibited a much higher output than the D-CTS/D-PDMS D-NG. In fact, a power density enhancement of more than 11-fold was achieved and was attributed to the highly porous structure as well as the high surface area exhibited by the P-CTS and P-PDMS films. It is worth noting that the P-CTS/P-PDMS A-NG generated a higher output than that of the P-CNF/P-PDMS A-NG (i.e., 30.0 V vs 22.3 V and 3.4 μA vs 2.2 μA), which can be attributed to the amino groups present on the glucosamine units of CTS. Amino groups are excellent electron-donors,[31] giving the CTS higher tribopositive polarity compared to CNF, thus leading to a higher output.

On the basis of the results discussed above, the triboelectric output performance of the TENG can be effectively improved by introducing a porous structure, which may be attributed to the higher surface area. Porous polymer films can increase the contact area upon compressing, generate more charges,[37] and thus increase the output power in the A-NG. Furthermore, additional charges can also be generated on the porous surfaces of the pores by electrostatic induction (Figure 4).[37] In order to further demonstrate the importance of the highly porous structure, we measured the output voltage and current of the A-NG fabricated using porous CNF and CTS aerogel films paired with P-PI films of varying porosities. As shown in **Figure 5**a,b, the output voltage and current of P-CNF/P-PI A-NGs increased from 22.1 V and 2.4 μA to 27.9 V and 3.4 μA, and then to 39.3 V and 4.3 μA, when the porosity of P-PI increased from 78% to 84%, and then 92%, respectively. Similarly, the output performance of P-CTS/P-PI A-NGs also increased significantly with the increasing porosity of PI (Figure 5c,d). Remarkably, the A-NG fabricated using the P-CTS aerogel and the 92% porous PI aerogel (P-PI92) with a BET surface area of 212 $m^2\ g^{-1}$ demonstrated very stable and high outputs; namely, an open-circuit voltage (V_{oc}) of 60.6 V and a short-circuit current (I_{sc}) of 7.7 μA, corresponding to a power density of 2.33 W m^{-2}, which is attributed to the increase of the contact area as well as electrostatic induction in the porous structure.

The following tests were conducted on the P-CTS/P-PI92 A-NG because of its superior performance. To investigate the output performance of the P-CTS/P-PI92 A-NG to external loads, the A-NG was connected to resistors with different resistance values (10^3–10^7 Ω). As shown in **Figure 6**a, the output voltage through the external resistor increased gradually with increasing resistance and reached a high value of 56 V at a high resistance of 10^7 Ω. The instantaneous output powers ($W = V^2_{oc}/R$) on the external load by the P-CTS/P-PI92 A-NG were also calculated and plotted in Figure 6a, which shows that the output power density reached a peak value of 4.50 W m^{-2} at a resistance of 1 MΩ. Such a high output power is sufficient to drive many small

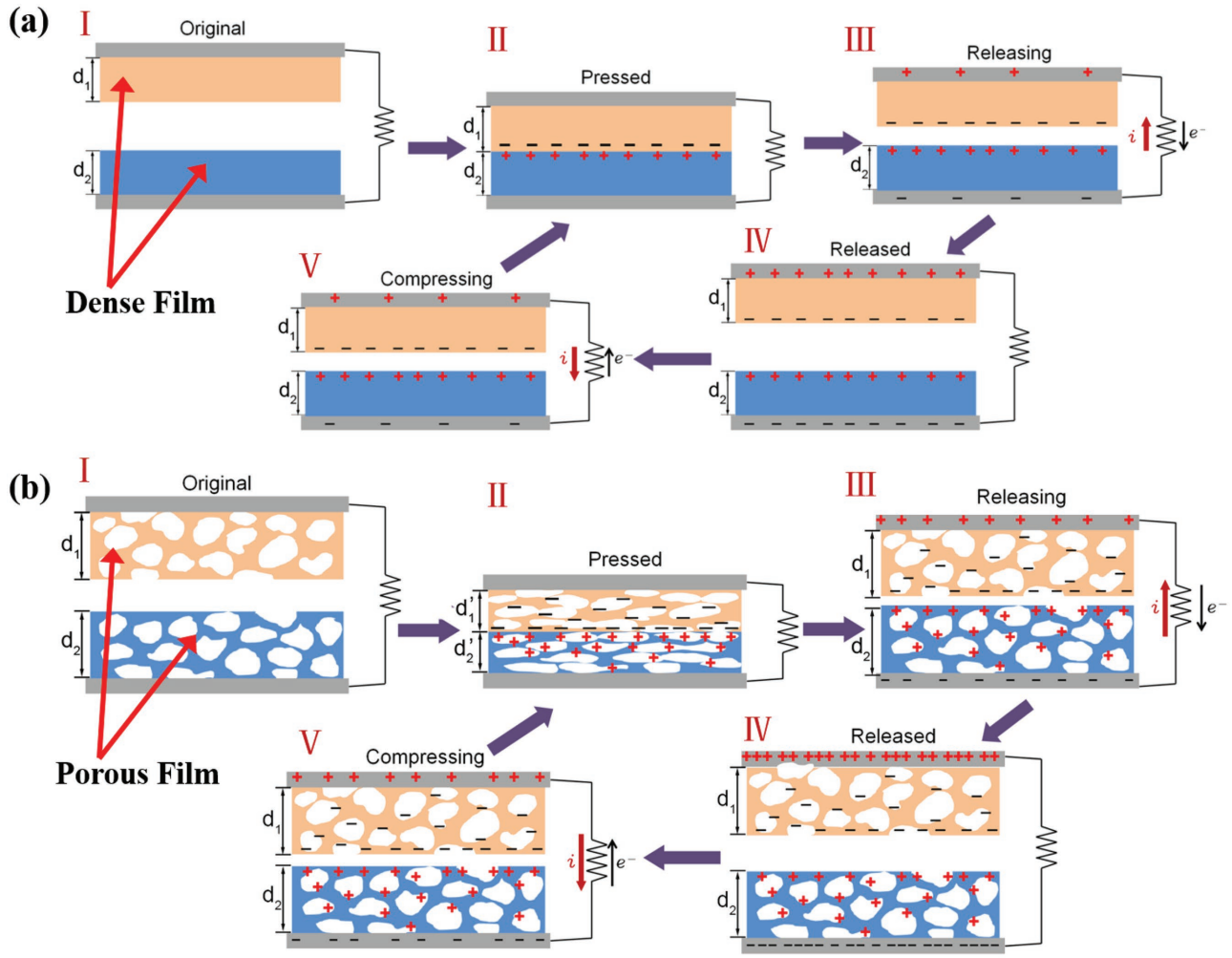

Figure 4. Schematic illustration of the operating principle of the a) D-NG and b) A-NG.

electronic devices and charge energy storage devices. For demonstration purposes, the P-CTS/P-PI92 A-NG was connected to 22 blue light-emitting-diodes (LED) through a commercial bridge rectifier. It can be seen that 22 blue LEDs (with a turn-on voltage of about 2.6 V for each) connected in series, which spell the letters "ANG", were instantly turned on by the A-NG once it was subjected to an external stress (Figure 6b and Video S1, Supporting Information). To further demonstrate the A-NG as an efficient energy harvesting power source, it was used to charge a capacitor (22 μF) through a bridge rectifier. As shown in Figure 6c, it charged the capacitor to ≈4.0 V within 600 s.

The cyclic stability, which is an important parameter for A-NG, was evaluated by continuously testing for 10 000 cycles at a frequency of 10 Hz as shown in Figure 6d. The output voltage signals of the A-NG revealed no obvious change after 10 000 cycles. Furthermore, the output voltage did not deteriorate even if the A-NG device was measured again after one or two months (Figure 6e). These experimental data suggest that A-NGs fabricated using porous polymer film possessed superior stability and reliability.

There are abundant hydroxyl groups on the glucose units of cellulose that allow for various surface functionalizations[40,41] to tune the dielectric and triboelectric properties of cellulose. Due to the relatively low triboelectric positive polarity possessed by CNF,[29] the TENGs fabricated using CNF as the triboelectric positive layer yielded lower triboelectric outputs than those using CTS. Therefore, amino groups, which have excellent electron-donating functionality, were introduced to the CNF aerogels via silanization (aminosilane) using a simple thermal chemical vapor deposition (CVD) process to increase the positive polarity of CNFs (**Figure 7**a).[32,42] Successful silanization of the porous CNF aerogels was confirmed by fourier-transform infrared spectroscopy (FTIR) analysis (Figure S3, Supporting Information). The absorption bands at ≈795 and ≈1261 cm^{-1} were ascribed to the characteristic vibrations of Si—O—Si and C—Si asymmetric stretching in C—Si—O units, respectively, suggesting that the amino groups were successfully grafted to the glucose units of CNF.[42]

Aminosilane-functionalized P-CNF aerogel film (AS-P-CNF) was used as a positive layer paired with P-PI92 to assemble the AS-P-CNF/P-PI92 A-NG. As shown in Figure 7b,c, the AS-P-CNF/P-PI92 A-NG delivered an output voltage of 57.2 V and an output current of 8.6 μA, which was much higher than that of the P-CNF/P-PI92 A-NG (i.e., 39.3 V and 4.3 μA),

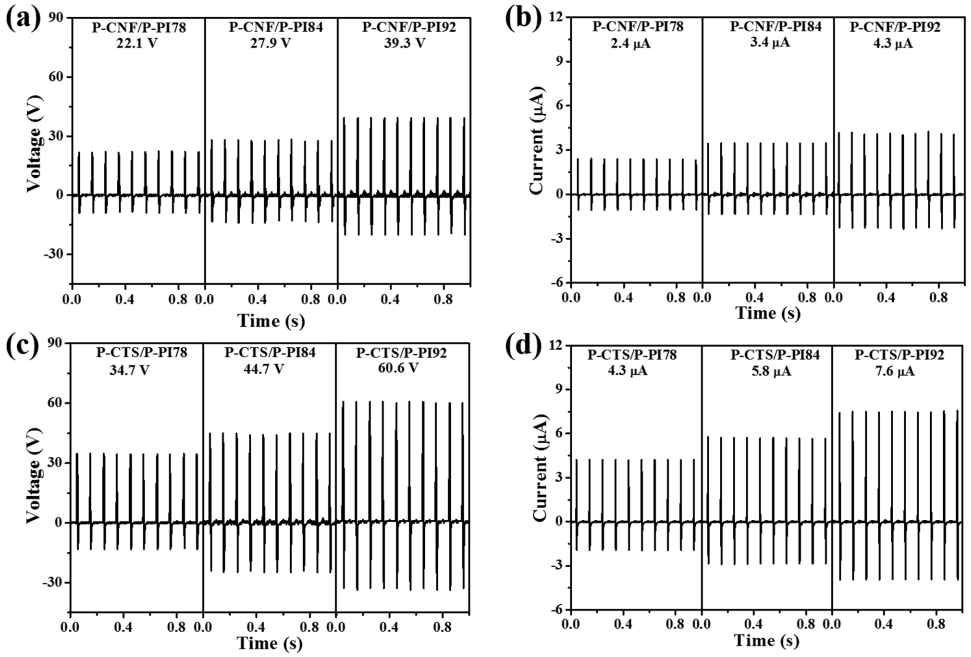

Figure 5. Output a) voltage and b) current of the A-NG fabricated using P-CNF aerogel film paired with various P-PI aerogel films with varying porosities; output c) voltage and d) current of the A-NG fabricated using P-CTS aerogel film paired with various P-PI aerogel films with varying porosities.

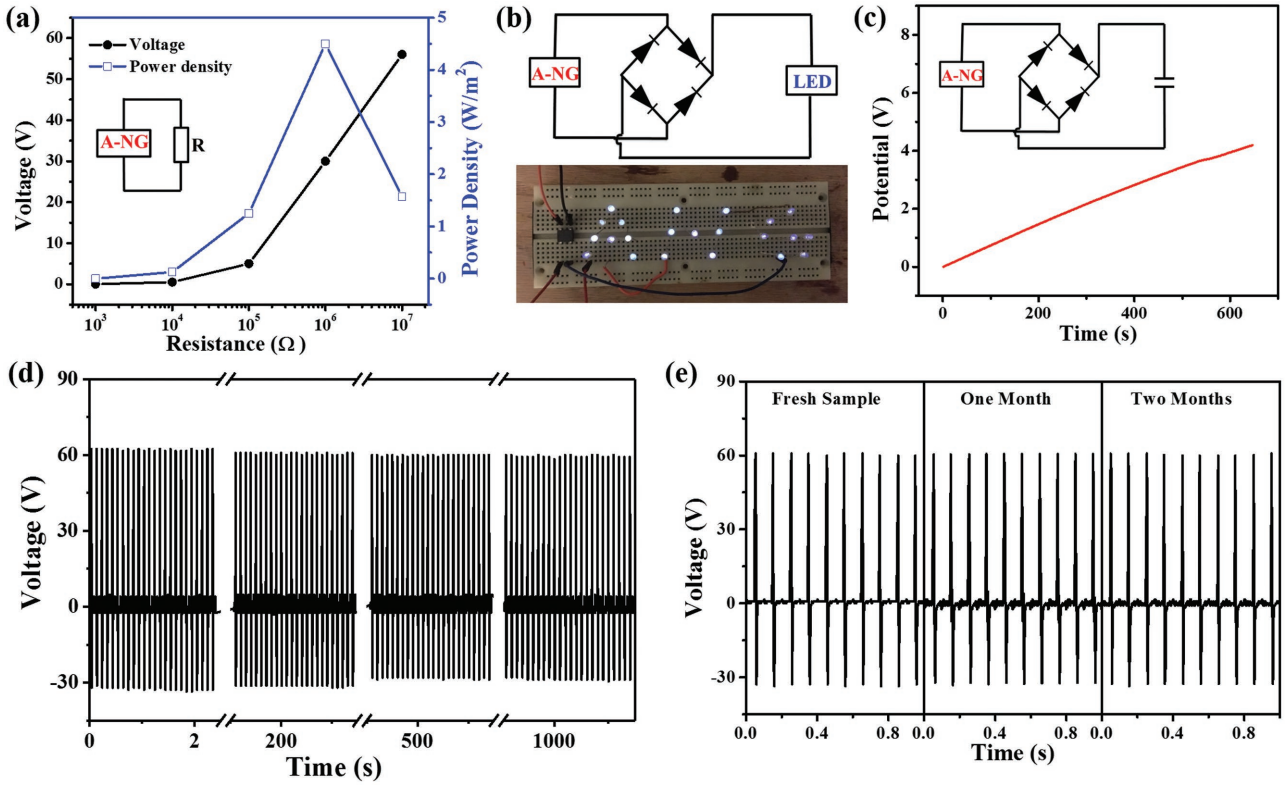

Figure 6. The output performance and stability of the P-CTS/P-PI92 A-NG. a) Output voltage and instantaneous power density as a function of load resistance. The inset shows the equivalent circuit. b) Twenty-two blue LEDs were instantly turned on by the A-NG under a compressive stress of 0.03 MPa at a frequency of 20 Hz. c) The charging curve of a capacitor by the A-NG under a compressive stress of 0.03 MPa at a frequency of 20 Hz. d) Durability performance of the A-NG tested for 10 000 cycles. e) Stability test for the A-NG directly after fabrication and one month, and two months after fabrication.

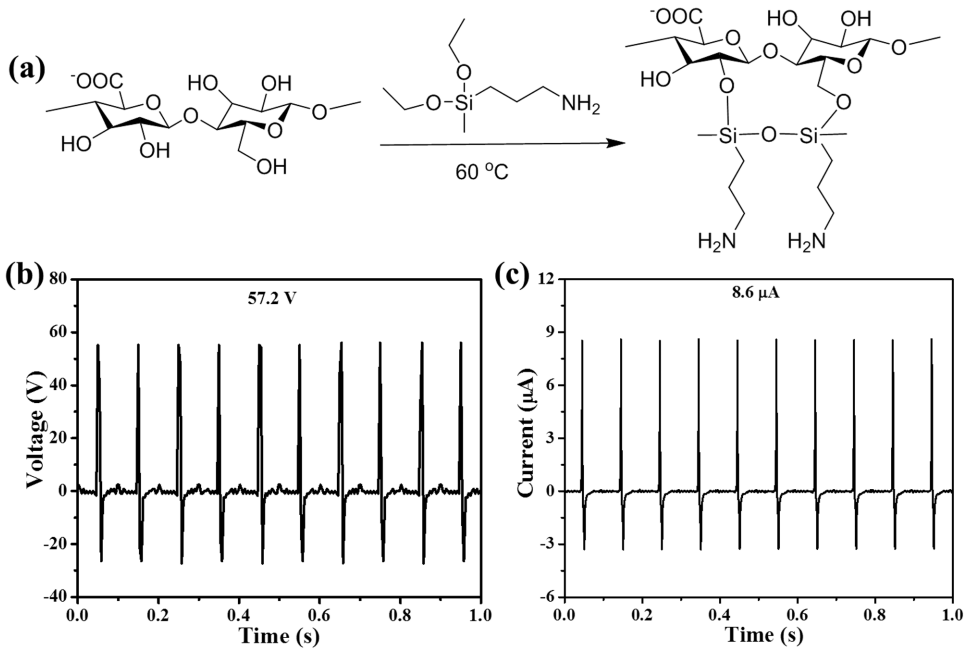

Figure 7. a) Schematic illustration of the surface modification of the CNF aerogel with aminosilane. Output b) voltage and c) current of the AS-P-CNF/P-PI92 A-NG.

corresponding to a threefold power density enhancement. These results demonstrated that the tribopositive polarity of cellulose can be improved via functionalization of cellulose with amine, which leads to a dramatically enhanced TENG output performance. Furthermore, this experiment demonstrates the great potential of tuning the tribopolarity of renewable, biocompatible, and biodegradable polysaccharides via silanization through a simple thermal chemical vapor deposition process, which can be used to fabricate high performance TENGs.

3. Conclusions

A novel class of high performance polymer A-NGs using highly porous polymer films as both triboelectric positive and negative layers has been demonstrated. P-CNF/P-PDMS and P-CTS/P-PDMS A-NGs exhibited a high output voltage and current of 22.3 V and 2.2 μA, and 30.0 V and 3.4 μA, respectively, and resulted in more than an 8-fold and 11-fold power enhancement, respectively, compared to their corresponding D-NGs under the same mechanical stress. Furthermore, the effects of the aerogel porosity on the triboelectric output performance of A-NGs were investigated using P-CNF and P-CTS aerogel films paired with P-PI aerogel films of varied porosities. The triboelectric output performance of the A-NGs increased with increasing porosity, which was attributed to an increase in contact area as well as electrostatic induction in the porous structure. In addition, it was demonstrated that the tribopositive polarity of cellulose can be improved via surface functionalization of cellulose with aminosilane, leading to a dramatically enhanced TENG output performance. Thus, this research provides a simple, cost-efficient, and scalable method for fabricating high performance, biocompatible TENGs and will also provide new insights into designing new materials to advance energy harvesting devices.

4. Experimental Section

Preparation of P-CNF Aerogel Film: P-CNF aerogel was prepared by freezing CNF solution (17 mL, 0.90 wt%) in aluminum pans (diameter: 5.80 cm) in a dry ice–acetone solution at −78 °C followed by a freeze-drying process as previously reported.[25,32] The P-CNF aerogel film was obtained by compressing the P-CNF aerogel at a pressure of 1.0 MPa. For comparison, D-CNF films were prepared by film casting and were dried under natural convection conditions in a fume hood.

Preparation of AS-P-CNF Aerogel Film: A thermal CVD method was developed for the surface functionalization of the CNF aerogel.[32,42] Briefly, a glass vial containing 3-aminopropyl diethoxymethylsilane (1 mL, ≥97.0%, TCI America) was placed in a vacuum desiccator together with the CNF aerogels. The dessiccator was well sealed and vacuumed and heated in an oven at 60 °C for 48 h to obtain the AS-P-CNF aerogel. Thereafter, nitrogen was blown into the desiccator to remove any unreacted silane and by-products. The AS-P-CNF aerogel film was obtained by compressing the AS-P-CNF aerogel at a pressure of 1.0 MPa. The weight of the aerogel increased by 10 wt%.

Preparation of P-CTS Aerogel Film: CTS (M_w: 190–310 kDa, Sigma-Aldrich) (0.400 g) was dissolved in 40 mL of water with the addition of acetic acid (0.4 mL) to prepare the CTS solution (1.0 wt%). The P-CTS aerogel was obtained after freeze-drying the CTS solution (15 mL). The P-CTS aerogel was compressed into an aerogel film under a pressure of 1.0 MPa. For comparison, D-CTS films were prepared by film casting and were dried under natural convection conditions in the fume hood.

Preparation of P-PDMS Sponge: P-PDMS sponge was prepared using a solvent evaporation-induced phase-separation method. Briefly, a PDMS solution was prepared by mixing a PDMS prepolymer, curing agent (Sygard 184, Dow Corning), mineral oil, hexane, and sorbitan monooleate at a ratio of 10:1:8:22:0.1. The above solution was poured into petri dishes and left in a fume hood for 2 h to allow

the hexane to evaporate. Subsequently, it was cured at 100 °C for 1 h. The resulting film was immersed in hexane for 4 d to extract the mineral oil. The hexane solvent was changed every day. After that, the P-PDMS sponge was obtained after being soaked in succession in ethanol and water, followed by drying at ambient temperature. For comparison, a dense PDMS (D-PDMS) film was obtained by casting a PDMS prepolymer and curing agent mixture (without any solvent) at a 10:1 ratio.

Preparation of P-PI Aerogel Film: A PI aerogel film with a porosity of 92% (P-PI92) was synthesized by crosslinking BPDA with 50% DMBZ and 50% ODA, followed by supercritical drying as previously described.[36] The two porous PI aerogel films with porosities of 78% and 84%, termed P-PI78 and P-PI84, respectively, were obtained from the same PI gel as prepared above but by air drying at room temperature for 15 and 4 d, respectively, followed by vacuum drying at 75 °C overnight.

Fabrication of Porous Polymer A-NGs: All of the A-NGs fabricated in this work were based on the traditional vertical contact-separation mode, and all of the films were cut into 1 cm × 2 cm rectangles. P-CNF/P-PDMS A-NGs were fabricated as follows. P-CNF aerogel film and P-PDMS film were attached to the center of two ITO/PET substrates (2.5 cm × 5 cm, surface resistivity of 60 Ω sq^{-1}) separately, which served as the tribopositive and tribonegative layer, respectively. These two layers were assembled face-to-face and were separated by 2 mm PDMS spacers. Thereafter, the as-fabricated A-NG was connected to an external circuit through aluminum foil affixed to the ITO side of the substrates. For comparison, D-NGs were fabricated following the same procedure.

Characterization of Materials and TENGs: The densities of the various porous films, including P-CNF, P-CTS, P-PDMS, and P-PI, were calculated by measuring the mass and volume of the porous films. The microstructures of the various porous films were studied using a SEM (LEO GEMINI 1530). The porous films were treated using gold sputtering. The FTIR spectra of the CNF aerogels with and without aminosilane functionalization were recorded on a Tensor 27 spectrometer (Bruker, USA) with a 4 cm^{-1} resolution at room temperature. The BET specific surface area was determined by N_2 physisorption using a Gemini analyzer (Micromeritics, USA) by analyzing the amount of N_2 gas adsorbed on the samples with a relative vapor pressure (P/P_0) ranging from 0.05 to 0.3 at −196 °C. For the triboelectric output measurements of TENGs, the bottom electrode was fixed on a wood bench while the top electrode was compressed by a shaker (LDS V201, Brüel and Kjær, Denmark) with controlled force and frequency. The electrical output signals of the generators were recorded using an oscilloscope (DS1102E, Rigol, China) and a potentiostat (versaSTAT-3, Princeton Applied Research, USA). All tests described in the paper were done at least in triplicate and the most representative curves and results were reported.

Supporting Information

Supporting information is available from the Wiley Online Library or from the author.

Acknowledgements

Q.Z. and L.F. contributed equally to this work. The authors gratefully acknowledge the financial support of the University of Wisconsin–Madison and the China Scholarship Council (CSC).

Conflict of Interest

The authors declare no conflict of interest.

Keywords

aminosilane functionalization, energy harvesting, porous polymer films, triboelectric nanogenerators

Received: November 2, 2017
Revised: December 19, 2017
Published online:

[1] A. Midilli, M. Ay, I. Dincer, M. A. Rosen, *Renewable Sustainable Energy Rev.* **2005**, *9*, 255.
[2] F. R. Fan, W. Tang, Z. L. Wang, *Adv. Mater.* **2016**, *28*, 4283.
[3] J.-H. Lee, K. Y. Lee, M. K. Gupta, T. Y. Kim, D.-Y. Lee, J. Oh, C. Ryu, W. J. Yoo, C.-Y. Kang, S.-J. Yoon, J.-B. Yoo, S.-W. Kim, *Adv. Mater.* **2014**, *26*, 765.
[4] Y. Yang, W. Guo, K. C. Pradel, G. Zhu, Y. Zhou, Y. Zhang, Y. Hu, L. Lin, Z. L. Wang, *Nano Lett.* **2012**, *12*, 2833.
[5] X. Wang, J. Song, J. Liu, Z. L. Wang, *Science* **2007**, *316*, 102.
[6] Z. L. Wang, *ACS Nano* **2013**, *7*, 9533.
[7] X. Cao, Y. Jie, N. Wang, Z. L. Wang, *Adv. Energy Mater.* **2016**, *6*, 1600665.
[8] J. Peng, H. Zhang, Q. Zheng, C. M. Clemons, R. C. Sabo, S. Gong, Z. Ma, L.-S. Turng, *Nanoscale* **2017**, *9*, 1428.
[9] F. R. Fan, J. Luo, W. Tang, C. Li, C. Zhang, Z. Tian, Z. L. Wang, *J. Mater. Chem. A* **2014**, *2*, 13219.
[10] Y. H. Ko, G. Nagaraju, S. H. Lee, J. S. Yu, *ACS Appl. Mater. Interfaces* **2014**, *6*, 6631.
[11] L. Lin, Y. Xie, S. Niu, S. Wang, P.-K. Yang, Z. L. Wang, *ACS Nano* **2015**, *9*, 922.
[12] Z. L. Wang, J. Chen, L. Lin, *Energy Environ. Sci.* **2015**, *8*, 2250.
[13] C. Yao, A. Hernandez, Y. Yu, Z. Cai, X. Wang, *Nano Energy* **2016**, *30*, 103.
[14] F.-R. Fan, Z.-Q. Tian, Z. Lin Wang, *Nano Energy* **2012**, *1*, 328.
[15] J. Wang, Z. Wen, Y. Zi, P. Zhou, J. Lin, H. Guo, Y. Xu, Z. L. Wang, *Adv. Funct. Mater.* **2016**, *26*, 1070.
[16] K. Dong, J. Deng, Y. Zi, Y.-C. Wang, C. Xu, H. Zou, W. Ding, Y. Dai, B. Gu, B. Sun, Z. L. Wang, *Adv. Mater.* **2017**, *29*, 1702648.
[17] Y. Yang, H. Zhang, R. Liu, X. Wen, T.-C. Hou, Z. L. Wang, *Adv. Energy Mater.* **2013**, *3*, 1563.
[18] M. Wang, W. Li, C. You, Q. Wang, X. Zeng, M. Chen, *RSC Adv.* **2017**, *7*, 6772.
[19] H.-J. Kim, E.-C. Yim, J.-H. Kim, S.-J. Kim, J.-Y. Park, I.-K. Oh, *Nano Energy* **2017**, *33*, 130.
[20] J. Wang, Z. Wen, Y. Zi, L. Lin, C. Wu, H. Guo, Y. Xi, Y. Xu, Z. L. Wang, *Adv. Funct. Mater.* **2016**, *26*, 3542.
[21] D. Klemm, B. Heublein, H.-P. Fink, A. Bohn, *Angew. Chem., Int. Ed.* **2005**, *44*, 3358.
[22] D. Klemm, F. Kramer, S. Moritz, T. Lindström, M. Ankerfors, D. Gray, A. Dorris, *Angew. Chem., Int. Ed.* **2011**, *50*, 5438.
[23] R. J. Moon, A. Martini, J. Nairn, J. Simonsen, J. Youngblood, *Chem. Soc. Rev.* **2011**, *40*, 3941.
[24] Q. Zheng, H. Zhang, H. Mi, Z. Cai, Z. Ma, S. Gong, *Nano Energy* **2016**, *26*, 504.
[25] Q. Zheng, Z. Cai, Z. Ma, S. Gong, *ACS Appl. Mater. Interfaces* **2015**, *7*, 3263.
[26] Q. Zheng, A. Kvit, Z. Cai, Z. Ma, S. Gong, *J. Mater. Chem. A* **2017**, *5*, 12528.
[27] X. Du, Z. Zhang, W. Liu, Y. Deng, *Nano Energy* **2017**, *35*, 299.
[28] M. M. Alam, D. Mandal, *ACS Appl. Mater. Interfaces* **2016**, *8*, 1555.
[29] C. Yao, X. Yin, Y. Yu, Z. Cai, X. Wang, *Adv. Funct. Mater.* **2017**, *27*, 1700794.
[30] M. N. V. Ravi Kumar, *React. Funct. Polym.* **2000**, *46*, 1.

[31] H.-I. Lu, C.-W. Lu, Y.-C. Lee, H.-W. Lin, L.-Y. Lin, F. Lin, J.-H. Chang, C.-I. Wu, K.-T. Wong, *Chem. Mater.* **2014**, *26*, 4361.
[32] Q. Zheng, Z. Cai, S. Gong, *J. Mater. Chem. A* **2014**, *2*, 3110.
[33] Q. Zheng, A. Javadi, R. Sabo, Z. Cai, S. Gong, *RSC Adv.* **2013**, *3*, 20816.
[34] Y. Tang, Q. Zheng, B. Chen, Z. Ma, S. Gong, *Nano Energy* **2017**, *38*, 401.
[35] J. Zhao, G. Luo, J. Wu, H. Xia, *ACS Appl. Mater. Interfaces* **2013**, *5*, 2040.
[36] H. Guo, M. A. B. Meador, L. McCorkle, D. J. Quade, J. Guo, B. Hamilton, M. Cakmak, *ACS Appl. Mater. Interfaces* **2012**, *4*, 5422.
[37] K. Y. Lee, J. Chun, J.-H. Lee, K. N. Kim, N.-R. Kang, J.-Y. Kim, M. H. Kim, K.-S. Shin, M. K. Gupta, J. M. Baik, S.-W. Kim, *Adv. Mater.* **2014**, *26*, 5037.
[38] D. Jang, Y. Kim, T. Y. Kim, K. Koh, U. Jeong, J. Cho, *Nano Energy* **2016**, *20*, 283.
[39] X. He, X. Mu, Q. Wen, Z. Wen, J. Yang, C. Hu, H. Shi, *Nano Res.* **2016**, *9*, 3714.
[40] M. Isik, H. Sardon, D. Mecerreyes, *Int. J. Mol. Sci.* **2014**, *15*, 11922.
[41] S. Saini, M. N. Belgacem, M.-C. B. Salon, J. Bras, *Cellulose* **2016**, *23*, 795.
[42] T. Zhai, Q. Zheng, Z. Cai, L.-S. Turng, H. Xia, S. Gong, *ACS Appl. Mater. Interfaces* **2015**, *7*, 7436.